THE GEOLOGICAL SOCIETY OF AMERICA®

The Capitanian (Guadalupian, Middle Permian) mass extinction in NW Pangea (Borup Fiord, Arctic Canada): A global crisis driven by volcanism and anoxia

David P.G. Bond[1†], Paul B. Wignall[2], and Stephen E. Grasby[3,4]
[1]*Department of Geography, Geology and Environment, University of Hull, Hull, HU6 7RX, UK*
[2]*School of Earth and Environment, University of Leeds, Leeds, LS2 9JT, UK*
[3]*Geological Survey of Canada, 3303 33rd Street N.W., Calgary, Alberta, T2L 2A7, Canada*
[4]*Department of Geoscience, University of Calgary, 2500 University Drive N.W., Calgary Alberta, T2N 1N4, Canada*

ABSTRACT

Until recently, the biotic crisis that occurred within the Capitanian Stage (Middle Permian, ca. 262 Ma) was known only from equatorial (Tethyan) latitudes, and its global extent was poorly resolved. The discovery of a Boreal Capitanian crisis in Spitsbergen, with losses of similar magnitude to those in low latitudes, indicated that the event was geographically widespread, but further non-Tethyan records are needed to confirm this as a true mass extinction. The cause of this crisis is similarly controversial: While the temporal coincidence of the extinction and the onset of volcanism in the Emeishan large igneous province in China provides a clear link between those phenomena, the proximal kill mechanism is unclear. Here, we present an integrated fossil, pyrite framboid, and geochemical study of the Middle to Late Permian section of the Sverdrup Basin at Borup Fiord, Ellesmere Island, Arctic Canada. As in Spitsbergen, the Capitanian extinction is recorded by brachiopods in a chert/limestone succession 30–40 m below the Permian-Triassic boundary. The extinction level shows elevated concentrations of redox-sensitive trace metals (Mo, V, U, Mn), and contemporary pyrite framboid populations are dominated by small individuals, suggestive of a causal role for anoxia in the wider Boreal crisis. Mercury concentrations—a proxy for volcanism—are generally low throughout the succession but are elevated at the extinction level, and this spike withstands normalization to total organic carbon, total sulfur, and aluminum. We suggest this is the smoking gun of eruptions in the distant Emeishan large igneous province, which drove high-latitude anoxia via global warming. Although the global Capitanian extinction might have had different regional mechanisms, like the more famous extinction at the end of the Permian, each had its roots in large igneous province volcanism.

INTRODUCTION

The Capitanian (Guadalupian Series, Middle Permian) crisis is among the least understood of the major mass extinctions. It has been interpreted as extinction comparable to the "Big 5" Phanerozoic crises (Stanley and Yang, 1994; Bond et al., 2010a, 2015; Stanley, 2016) or, alternatively, as a gradually attained low point in Permian diversity of regional extent and therefore not a mass extinction at all (Yang et al., 2000; Clapham et al., 2009; Payne and Clapham, 2012; Groves and Wang, 2013). Although there is no universally accepted definition of "mass extinction," key criteria include the following: A mass extinction should have significant impact on a range of biota, it should be of geologically short duration, and it should be of global extent. Until recently, most studies have focused on equatorial (Tethyan) records, especially those from South China, where fusulinacean foraminifers and brachiopods lost 82% and 87% of species, respectively (Jin et al., 1994; Shen and Shi, 1996; Bond et al., 2010a), thus fulfilling the first criterion. These losses were originally ascribed to the Guadalupian-Lopingian Series boundary (end of Capitanian Stage), hence the widespread use of the term "end-Guadalupian extinction" in earlier literature. However, the South China benthic crisis has now been accurately dated to the *Jinogondolella altudaensis–Jinogondolella prexuanhanensis* conodont zones (Shen and Shi, 2009; Wignall et al., 2009a, 2009b; Bond et al., 2010a, 2010b), making this a mid-Capitanian crisis of short duration, fulfilling the second criterion. Several other marine groups were badly affected in equatorial eastern Tethys Ocean, including corals, bryozoans, and giant alatoconchid bivalves (e.g., Wang and Sugiyama, 2000; Weidlich, 2002; Bond et al., 2010a; Chen et al., 2018). In contrast, pelagic elements of the fauna (ammonoids and conodonts) suffered a later, ecologically distinct, extinction crisis in the earliest Lopingian (Huang et al., 2019). Although a severe extinction of Capitanian brachiopods has been found in the Boreal sections of Spitsbergen (Bond et al., 2015), evaluation of the true geographic extent of the crisis requires more evidence from outside Tethys to resolve the third criterion.

The losses in China coincided with the onset of Emeishan large igneous province volcanism in the southwest of the country (Wignall et al., 2009a; Huang et al., 2019), suggesting a role for large igneous province activity. The recent development of mercury as a proxy for volcanism (Sanei et al., 2012) permits further evaluation of the large igneous province–extinction link in locations far removed from the site of volcanism.

Several large igneous province–driven kill mechanisms have been implicated in the Capitanian crisis, especially marine anoxia, which is implicated in numerous other mass extinction scenarios (see reviews in Wignall, 2001; Bond and Wignall, 2014; Bond and Grasby, 2017). Notably, the Capitanian losses in Spitsbergen coincided with a phase of benthic oxygen depletion (Bond et al., 2015). Other purported Capitanian extinction mechanisms include cooling (Isozaki et al., 2007), death-by-photosynthetic shutdown at the onset of volcanism (Bond et al., 2010a, 2010b), ocean acidification caused by volcanogenic CO_2 (McGhee et al., 2013), and

†d.bond@hull.ac.uk.

GSA Bulletin; May/June 2020; v. 132; no. 5/6; p. 931–942; https://doi.org/10.1130/B35281.1; 8 figures; 3 tables; published online 30 August 2019.

volcanogenic toxic metal poisoning (Grasby et al., 2015).

Thus, controversy surrounds whether the Capitanian crisis was a true global extinction and whether (and how) the Emeishan large igneous province was responsible. We address this with a new record from the Sverdrup Basin (Arctic Canada). Our study presents brachiopod range data from the Degerböls and Lindström Formations of Ellesmere Island, Permian-aged mixed spiculitic chert/carbonate units that formed on a cool, siliciclastic ramp in the Boreal Ocean (Embry, 1988; Embry and Beauchamp, 2008, 2019; Beauchamp et al., 2009). We assessed the role of redox changes during this interval using a combination of petrographic and geochemical approaches, and we further examined the link between these factors and the Emeishan large igneous province using the mercury proxy for volcanism. The precise ages of the Degerböls and Lindström Formations are unclear, and we investigated this through lithostratigraphic and chemostratigraphic comparison with better-dated Boreal successions in East Greenland and Spitsbergen.

REGIONAL GEOLOGY

The rapidly subsiding Sverdrup Basin was infilled with up to 13 km of Carboniferous to Paleogene sediments. It extends ~1200 km east-west and 400 km north-south from present-day Ellesmere and Axel Heiberg Islands (Nunavut, Canadian High Arctic) in the northeast to Melville Island in the west (Fig. 1; Balkwill, 1978; Embry and Beauchamp, 2008). The basin margins lay to the west, south, and east of our study area on Ellesmere Island and opened to the north into the Boreal (Arctic) Ocean, although connection was likely limited by the presence of Crockerland, a structural high that formed the northern basin rim (Embry, 1988, 1989). The Middle to Late Permian succession at Borup Fiord (81°00′33.4″N, 81°30′51.0″W; Fig. 2) formed at around 40°N on a shallow, open-marine siliceous ramp near the basin's northeastern margin and belongs to the Degerböls and Lindström Formations (but shares lithological similarities with their more distal equivalents, the van Hauen and Black Stripe Formations, respectively; Beauchamp et al., 2009; Embry and Beauchamp, 2019). The succession is composed of white to pale-gray spiculitic cherts and numerous limestone interbeds (Beauchamp and Grasby, 2012). The Lindström Formation is overlain conformably by the latest Permian–Early Triassic Blind Fiord Formation (Grasby and Beauchamp, 2008; Proemse et al., 2013) at Borup Fiord, while an unconformity marks this contact in more proximal settings. As in other regions, notably the lithostratigraphically similar Svalbard and Barents Sea, the Permian-Triassic boundary lies a few meters above the major lithological change at the formational contact (Beauchamp et al., 2009). The Blind Fiord Formation is a thick succession of offshore mudstones, siltstones, and shelf-slope sandstones that record major flooding, as well as the famous Permian-Triassic mass extinction, at its base (Embry, 1988; Embry and Beauchamp, 2008; Grasby and Beauchamp, 2008; Beauchamp et al., 2009).

The complete succession was uplifted during the Eurekan orogeny (the Paleogene convergence of Greenland and the Canadian Arctic; Harrison et al., 1999), and the resistant Permian outcrops are particularly well exposed in the poorly vegetated Arctic desert. The Degerböls and Lindström Formations thus preserve an excellent, but little-studied, archive of Permian environmental and biotic changes on the NW margin of Pangea.

MATERIAL AND METHODS

Facies and Fossils

Sedimentary logging was undertaken through ~100 m of the Degerböls and Lindström Formations and the basal meters of the Blind Fiord Formation at Borup Fiord, which was accessed by helicopter in July 2015. The outcrop lies alongside an east-west–trending glacier and provides a continuous exposure of fresh surfaces polished by ice movement. Facies, and trace and body fossils (principally brachiopods) were identified in the field. The field observations were supplemented with analysis of 24 thin sections.

Redox Proxies

The concentrations of redox-sensitive trace metals in marine sediment provide a measure of ancient depositional conditions, because the reduced forms of many metals (e.g., Mo, U, V, and Mn) are insoluble in seawater; therefore, these elements are scavenged by sediment under anoxic conditions. The U, Th, and K concentrations of individual beds were measured in the field for 3 min per bed using a Radiation Solutions RS-230 handheld gamma-ray spectrometer (Fig. 3) that assays a parabola of rock ~1 m in diameter. Forty-two samples (BF2 to BF43) were collected from the same levels for additional trace metal assays (a full suite, including Mo, Al, U, Th, V, and Mn), which were performed at Acme Laboratories, where powdered samples digested in a 2:2:1:1 acid solution of H_2O:HF:$HClO_4$:HNO_3 were analyzed using a PerkinElmer mass spectrometer with ±2% analytical error. Our mass

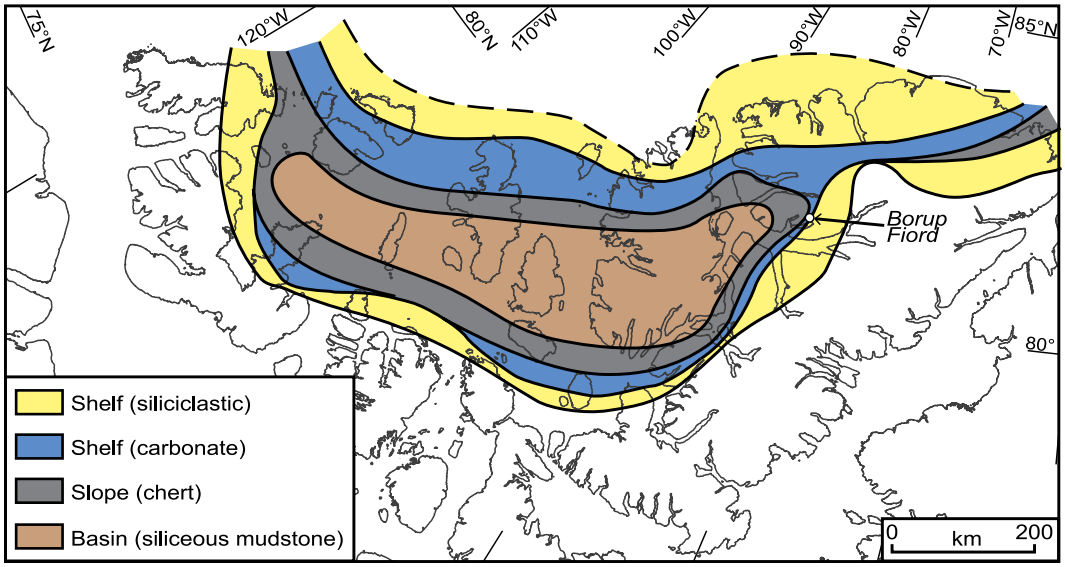

Figure 1. Regional paleogeography of the Sverdrup Basin in the Middle Permian (modified from Beauchamp and Grasby, 2012). The Borup Fiord section lies at the convergence of several facies on this map and records interbedded cherts and limestones.

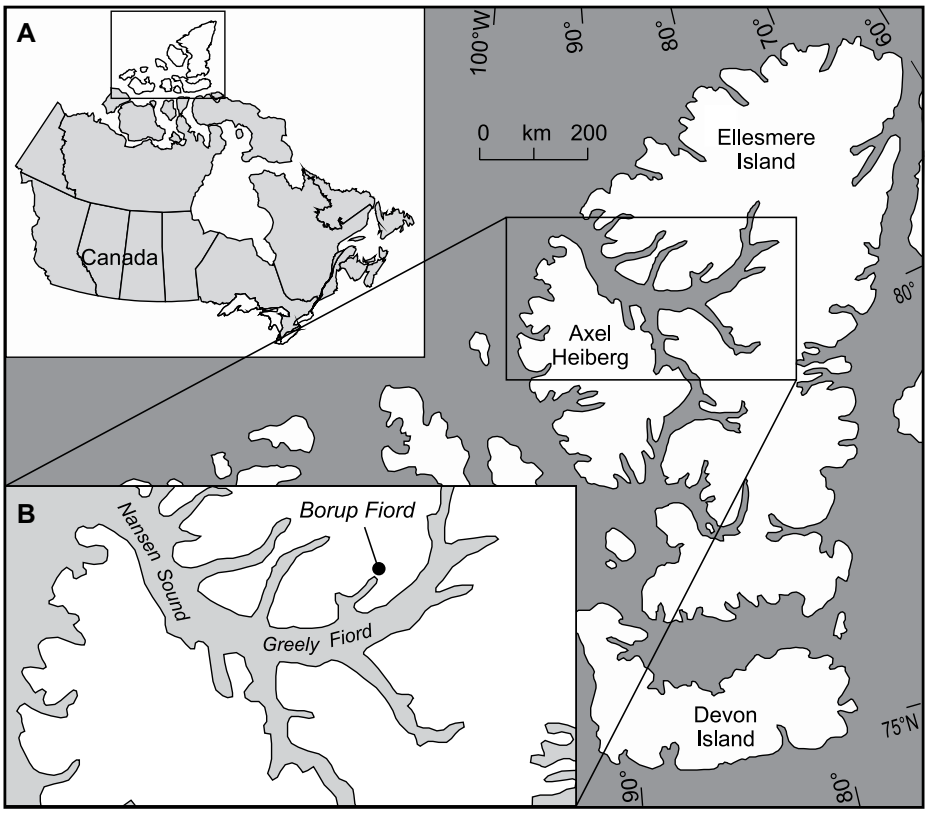

Figure 2. Location maps of the Borup Fiord section on Ellesmere Island within Arctic Canada.

Figure 3. Field photograph of the upper part of the Borup Fiord section, showing pale limestones of the upper Degerböls Formation (foreground) overlain by pale-gray and white cherts of the Lindström Formation. The instrument resting on the bedding plane (a Radiation Solutions RS-230 handheld gamma-ray spectrometer) rests on a surface that records the extinction level, marked by the last appearance of brachiopods including *Liosotella* sp. and *Linoproductus* sp.

spectrometry results provided an independent test of the validity of field-based, handheld gamma-ray spectrometry (Fig. 4).

Pyrite framboid analysis is a useful independent proxy for ancient redox conditions. In modern environments, pyrite framboids form in the narrow iron-reduction zone developed at the redox boundary, but they cease growing in the more intensely anoxic conditions of the underlying sulfate-reduction zone (Wilkin et al., 1996). During euxinic conditions (i.e., free H_2S occurs within the water column), framboids develop in the water column but are unable to achieve diameters much larger than 5 µm before they sink below the iron-reduction zone and cease to grow (Wilkin et al., 1996). Euxinia is therefore characterized by populations of tiny framboids with a narrow size range, whereas dysoxic or weakly oxygenated seafloors produce framboid populations that are larger and more variable in size (Bond and Wignall, 2010). Twenty-four field samples from Borup Fiord were examined using carbon-coated polished chips viewed in backscatter mode at a magnification of ~2500× on a Zeiss EVO-60 scanning electron microscope (SEM) at the University of Hull to determine the size distribution of pyrite framboids (where present). Where possible, at least 100 framboids were measured from each sample (levels bearing statistically robust numbers of pyrite framboids are shown on Fig. 4). Framboid size distributions were plotted with mean diameter versus standard deviation within each sample, which allowed a comparison of framboid populations in ancient sediments with modern euxinic, anoxic, and dysoxic populations.

Mercury, Total Organic Carbon, and Total Sulfur

Mercury (Hg) emissions associated with large igneous province emplacement were first recognized by Sanei et al. (2012), who identified a large Hg spike with probable origin in the eruptions of the Siberian Traps, i.e., the end-Permian killer. Mercury has since become a popular proxy for volcanism, and similar Hg anomalies are associated with other large igneous province events such as the Triassic–Jurassic Central Atlantic Magmatic Province (e.g., Thibodeau et al., 2016; Percival et al., 2017) and the Cretaceous–Paleogene Deccan Traps (e.g., Sial et al., 2013, 2014; Silva et al., 2013; Font et al., 2016). The 42 samples taken for trace metal analysis were analyzed for Hg at the Geological Survey of Canada (GSC) Atlantic facility using a LECO AMA254 mercury analyzer (±10%; Hall and Pelchat, 1997). Hg concentrations are typically normalized to total organic carbon (TOC) because of the propensity for Hg to bind to organic

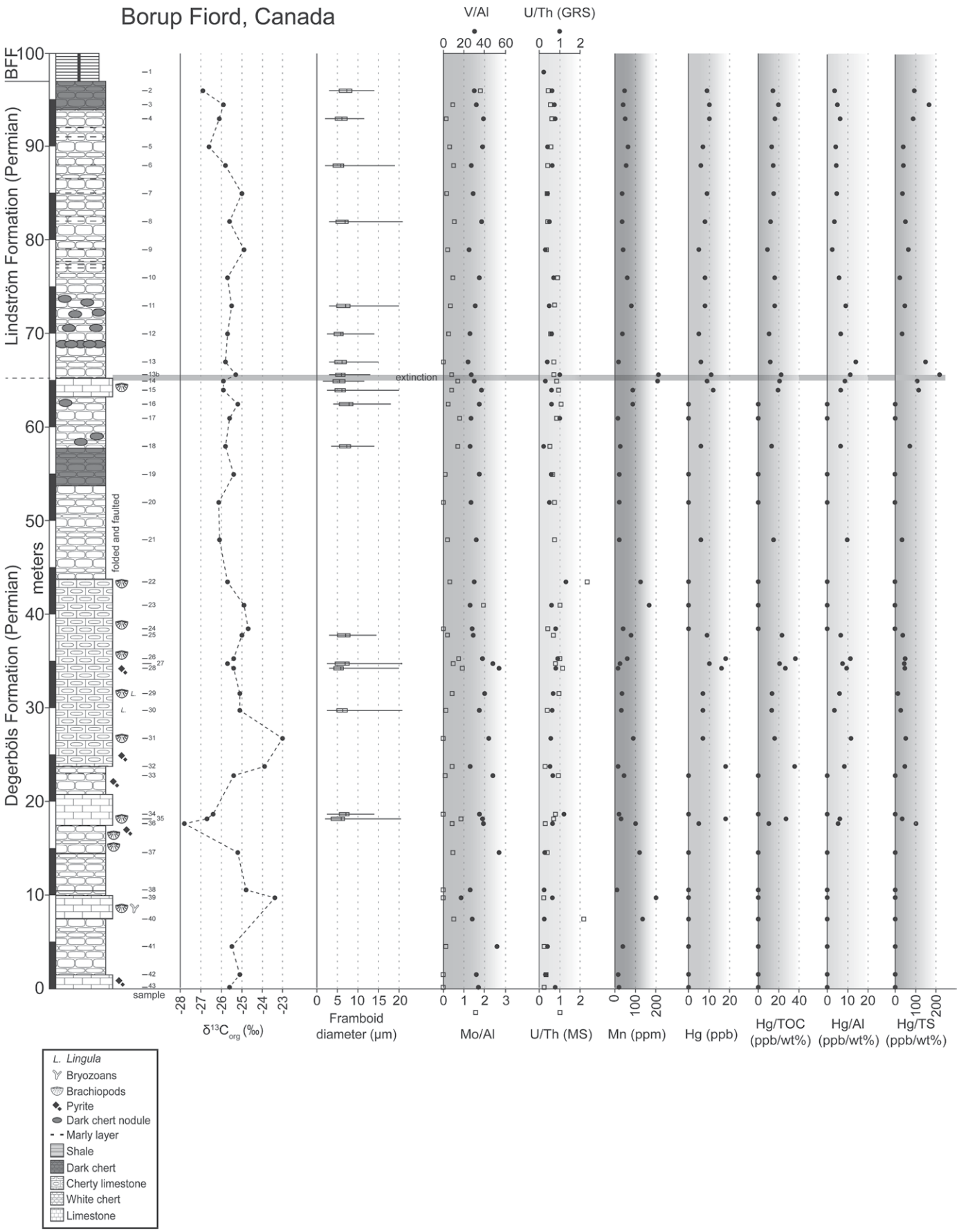

Figure 4. Log of the Borup Fiord section (81°00′33.4″N, 81°30′51.0″W, North American Datum 1983 [NAD83]), showing the upper part of the Degerböls Formation and the Lindström Formation up to the contact with the overlying Blind Fiord Formation (BFF) at 97 m height. The contact between the Middle Permian Degerböls Formation and the Upper Permian Lindström Formation is uncertain, but Beauchamp et al. (2009) considered an absence of carbonates to be diagnostic of the younger formation. The log shows lithologies, brachiopod-rich levels, sample positions, carbon isotope values ($\delta^{13}C_{org}$), pyrite framboid box-and-whisker plots, trace metal redox proxy data, and Hg concentrations. Pyrite framboid box-and-whisker plots show the 25th and 75th percentiles of framboid diameters in each sample (horizontal extent of black box), mean framboid diameter (central vertical line), and maximum and minimum framboid diameter (long horizontal line). The U/Th panel (yellow) was measured using in the field using a Radiation Solutions portable gamma-ray spectrometer (GRS; black circles), and in the laboratory by mass spectrometry (MS; open squares). There is remarkable correspondence between the two data sets, corroborating the application of field portable gamma-ray spectrometry. The extinction level (between samples 14 and 13b) is marked by populations of tiny pyrite framboids, and high V/Al and U/Th values, indicating that oxygen-poor conditions developed at this level. The concurrent marked increase in Mn concentrations is suggestive of proximity to sulfidic, deeper basinal waters (creating a "bathtub ring" of Mn at the redox boundary; Frakes and Bolton, 1984). The extinction level also records an increase in Hg concentrations that withstand normalization to total organic carbon (TOC), Al, and total sulfur (TS), which we interpret to be linked to distant volcanism in the Emeishan large igneous province. The biostratigraphically defined Permian-Triassic boundary lies a few meters above the Lindström–Blind Fiord formational contact at the top of our succession.

matter during sedimentation. We measured TOC at GSC-Calgary using Rock-Eval 6©, with ± 5% analytical error of reported value, based on repeats and reproducibility of standards run after every fifth sample (Lafargue et al., 1998). It is common practice to normalize Hg to TOC only where the latter exists in concentrations >0.2% (e.g., Grasby et al., 2016), since normalizing to smaller values magnifies errors to an unacceptable level. All of our samples had TOC >0.37%, and thus we normalized all of our Hg data to TOC. We also present Hg values normalized to both Al and total sulfur (TS), the concentrations of which were ascertained by mass spectrometry, for reasons discussed below.

Chemostratigraphy

The 42 samples taken for trace metal and Hg analysis were also analyzed for their organic carbon isotope ($\delta^{13}C_{org}$) values at the University of Calgary by continuous flow–elemental analysis–isotope ratio mass spectrometry, using a Finnigan Mat Delta + XL mass spectrometer interfaced with a Costech 4010 elemental analyzer, with standards run every fifth sample. Combined analytical and sampling error for $\delta^{13}C_{org}$ was ± 0.2‰ (1σ). Grasby et al. (2013) demonstrated a high degree of correspondence between carbon isotope records from the Sverdrup Basin and those from the Tethys and Neo-Tethys Oceans. As such, we can use chemostratigraphic correlation to relate our section to other Middle to Late Permian Boreal records (e.g., Spitsbergen), as well as to records from further afield (e.g., Tethys).

RESULTS

Facies and Fossils

The Degerböls Formation at Borup Fiord is dominated by pale cherts, limestones, and cherty limestones. The contact with the overlying Lindström Formation is uncertain, but Beauchamp et al. (2009) considered the latter to lack carbonates, and so we tentatively placed this formational contact at ~65 m section height (Fig. 4). The Lindström Formation cherts are abruptly succeeded by shales of the Blind Fiord Formation at the top of our studied section (Fig. 4). The lower 24 m of strata consist of interbedded pale-gray limestones and white cherts that are intensely burrowed by *Zoophycos*. Brachiopods, including *Costinifera arctica*, *Megousia weyprechti*, *Spiriferella* sp., and *Rhynchopora* sp., are common in both lithologies (Fig. 5A; Table 1), and bryozoans are seen on some limestone bedding surfaces. Pyrite is visible in the field at several levels (Fig. 4). These beds are overlain by 20 m of pale, cherty limestones that contain abundant brachiopods (the previously mentioned taxa, plus *Linoproductus* sp., *Neospirifer* sp., *Waagenoconcha* sp., and *Derbyia* sp.). The inarticulate brachiopod *Lingula freboldi* was also seen in abundance on bedding surfaces at BF30 and BF29 (Fig. 5B). Again, some levels were visibly pyritic.

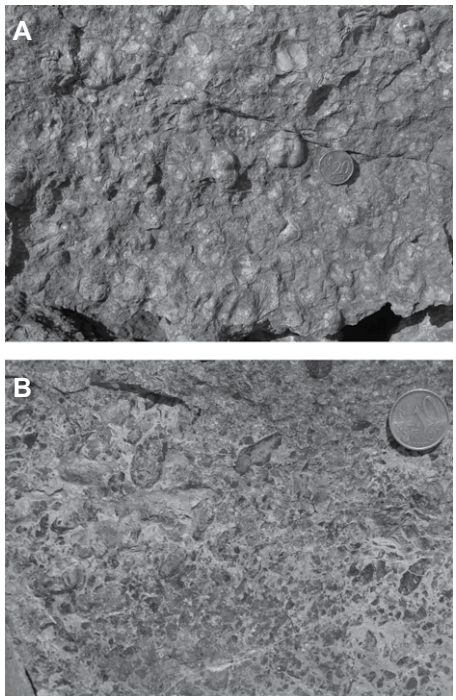

Figure 5. Field photographs showing (A) abundant brachiopods on a bedding surface at BF38 at Borup Fiord, where taxa include *Costinifera arctica*, *Spiriferella* sp., and *Rhynchopora* sp. (the coin is 22 mm in diameter); and (B) abundant *Lingula freboldi* on a bedding surface at BF29 (the coin is 20 mm in diameter).

The fossiliferous cherty limestones pass into 20 m of pure, spiculitic, white to dark-gray cherts that lack visible macrofossils. The interval between 54 m and 44 m section height is deformed, with some folding and small-scale faulting seen in the field. Brachiopods (*Linoproductus* sp. and *Liosotella* sp.) were observed again in our youngest Permian limestone, a 2-m-thick unit at around 65 m section height (samples BF15 and BF14). These were the last occurrences of brachiopods in the section, and so the extinction of brachiopods lies between BF14 and BF13b.

TABLE 1. BRACHIOPOD DISTRIBUTIONS IN THE DEGERBÖLS AND LINDSTRÖM FORMATIONS AT BORUP FIORD, ARCTIC CANADA

Sample	Taxa
BF14	*Linoproductus* sp., *Liosotella* sp.
BF23	*Linoproductus* sp., *Neospirifer* sp.
BF29	*Lingula freboldi*
BF30	*Derbyia* sp., *L. freboldi*
BF31	*Costinifera arctica*, *Megousia weyprechti*, *Waagenoconcha* sp.
BF36	*M. weyprechti*
BF38	*C. arctica*, *Rhyncopora* sp., *Spiriferella* sp.

Note: See Figure 4 for sample positions.

Above 65 m section height, the strata consist of 32 m of mostly white, spiculitic cherts (becoming dark gray in the uppermost meters) with occasional thin marly layers. Carbonates are absent from this part of the succession, which we ascribe to the Lindström Formation. Although shelly benthos was absent, some bedding planes in these cherts showed complex burrow networks (including *Planolites*, *Rosselia*, *Zoophycos*, and a trace resembling *Muensteria*; Figs. 6A and 6B). The dark cherts found in the topmost meters of the Lindström Formation are overlain by poorly exposed orange-weathering, pyritic, dark shales of the Blind Fiord Formation at 97 m section height. As in other regions in the Boreal Realm (e.g., Spitsbergen and Greenland), the Permian-Triassic boundary lies a few meters above this formational contact in Arctic Canada (Grasby and Beauchamp, 2008; Beauchamp et al., 2009).

Redox-Sensitive Trace Metals

The redox-sensitive trace metal ratios Mo/Al and V/Al reveal strikingly similar trends (Fig. 4), with the highest ratios (suggestive of poorly oxygenated conditions) occurring together between 20 m and 40 m section height and from ~60 m section height through to the top of the section. Peak Mo/Al and V/Al values are around 2 and 50, respectively. We calculated U/Th from data obtained by mass spectrometry as well as by field portable gamma-ray spectrometry (Table 2). The two data sets are in remarkably close accordance, corroborating the application of the field portable gamma-ray spectrometry tool. As with Mo/Al and V/Al, the highest ratios, of ~1, occur between 20 m and 45 m section height, and from ~60 m to 67 m (i.e., around the extinction interval; Fig. 4). The concentration of Mn at Borup Fiord is also of interest. The generally low values (<50 ppm Mn) seen in this sequence are interrupted by three intervals of elevated Mn concentrations (>100 ppm), from 8 m to 18 m (samples BF40 to BF36), 41 m to 43 m (BF23 and BF22), and finally precisely at the extinction level (65 m, BF14 and BF13b; Table 2). The highest Mn concentrations, >200 ppm, were found in these latter two samples.

Pyrite Framboids

Given the pale color of the chert and limestone facies, pyrite framboids are surprisingly common in the Borup Fiord samples (Table 3).

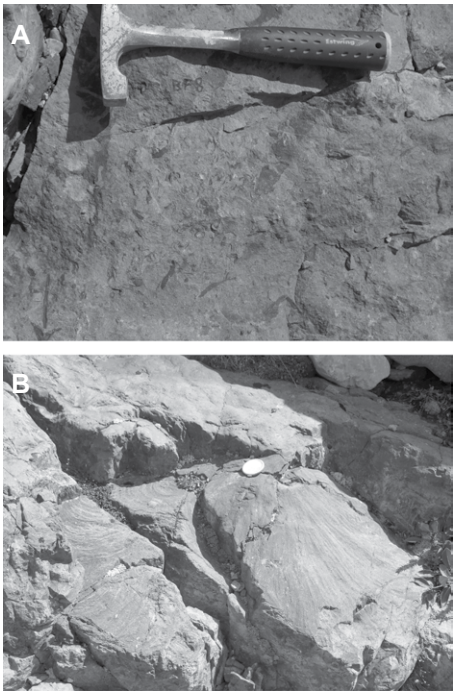

Figure 6. Field photographs showing (A) complex burrow networks on a bedding surface at BF8 (hammer for scale); and (B) *Zoophycos* traces on a bedding surface of chert near the top of the section (the lens cap is 5 cm in diameter).

TABLE 2. COMPILATION OF KEY GEOCHEMICAL DATA FROM THE DEGERBÖLS AND LINDSTRÖM FORMATIONS AT BORUP FIORD OBTAINED USING MASS SPECTROMETRY, PORTABLE GAMMA-RAY SPECTROMETRY, MERCURY ANALYZER, AND ROCKEVAL

Sample	Mo (ppm)*	Mn (ppm)*	Al (%)*	V (ppm)*	U (ppm)*	Th (ppm)*	U (ppm)†	Th (ppm)†	Hg (ppb)§	TOC (%)#	TS (%)*
BF2	4.5	48	2.52	75	2.2	5	3.2	5.1	9	0.65	0.1
BF3	0.9	40	2	64	2.4	4.4	4.1	5.6	10	0.51	0.06
BF4	0.2	50	1.53	60	2.1	3.4	4.9	6.2	10	0.60	0.11
BF5	0.5	64	1.68	64	2.8	4.9	1.4	3.3	7	0.53	0.18
BF6	0.7	55	1.43	39	1.5	3.6	3.9	6.2	6	0.44	0.16
BF7	0.3	35	1.9	56	1.5	3.8	1.8	4.3	9	0.60	0.25
BF8	1.2	35	2.27	83	1.9	4.5	2.1	4.1	8	0.66	0.16
BF8	0.4	36	2.19	55	1.2	3.3	1.5	4.3	5	0.58	0.08
BF9	0.6	61	1.36	47	1.8	2	2	2.9	8	0.49	0.38
BF10	0.3	78	0.88	27	1.2	1.6	1.5	2.9	8	0.43	0.17
BF11	0.2	36	0.8	21	0.8	1.4	1.3	2	5	0.60	0.16
BF12	<0.1	18	0.42	10	0.5	0.7	1.1	2.6	6	0.44	0.04
BF13	0.4	214	0.97	26	1.3	1.8	2.4	2.5	11	0.42	0.05
BF13b	0.7	210	1	30	1.6	1.9	1.1	3.4	9	0.44	0.08
BF14	0.7	86	1.74	64	3	3.2	2.4	3.9	12	0.49	0.1
BF15	0.2	87	0.83	29	1.8	1.7	1.6	2.9	<5	0.41	0.08
BF16	0.3	15	0.37	10	0.6	0.7	1.9	1.9	<5	0.37	0.02
BF17	0.6	25	0.88	23	0.8	1.5	0.7	3.1	6	0.44	0.08
BF18	0.1	21	1.48	52	1.6	2.4	1.5	2.5	<5	0.49	0.1
BF19	<0.1	21	0.52	14	0.9	1.2	1.7	3.7	<5	0.41	0.03
BF20	0.1	21	0.56	18	0.6	0.8	2.5	1.9	6	0.40	0.17
BF21	0.2	126	0.61	18	2.2	0.9	0.7	1.1	<5	0.50	0.19
BF22	0.6	166	0.31	8	0.5	0.5	3	3.6	<5	0.47	0.14
BF23	<0.1	39	0.29	8	0.3	0.7	8.7	10.1	<5	0.62	0.03
BF24	0.3	81	1.43	41	2.3	3.3	4.2	5.1	9	0.53	0.25
BF25	1.2	63	1.59	61	8	8.2	2.7	3.9	18	0.51	0.37
BF26	0.6	24	1.28	62	3.6	4.5	2.4	3.9	10	0.42	0.22
BF27	1.6	14	1.72	93	5.5	4.8	1.8	3.2	16	0.51	0.35
BF28	0.5	34	1.17	47	3	3.1	2.8	5.3	7	0.38	0.55
BF29	0.2	32	1.88	66	1.2	3	1.8	2.7	7	0.51	0.25
BF30	<0.1	89	0.57	25	2.2	0.7	4.1	3.4	7	0.66	0.13
BF31	0.9	15	2.18	57	1.7	5.6	1.9	2.9	18	0.50	0.39
BF32	0.1	44	1.3	63	2.5	2.7	0.5	1.8	<5	0.46	0.06
BF33	<0.1	21	2.01	71	2.7	3.4	0.4	1.7	<5	0.44	0.11
BF34	2.5	32	2.92	111	3.4	4.7	1.1	1.7	18	0.41	0.51
BF35	0.4	102	0.96	37	0.4	1.3	0.5	1.9	5	0.43	0.05
BF36	0.3	120	0.65	35	0.4	1	0.7	1.7	<5	0.50	<0.02
BF37	<0.1	11	0.23	6	<0.1	0.3	1	3.1	<5	0.40	<0.02
BF38	<0.1	200	0.65	11	0.2	0.9	2.2	2.8	<5	0.48	0.05
BF39	0.2	135	0.39	11	1.1	0.5	3.2	5.1	<5	0.65	0.05
BF40	0.1	38	0.85	44	0.4	1.6	4.1	5.6	<5	0.51	<0.02
BF41	<0.1	14	0.9	29	0.5	1.5	4.9	6.2	<5	0.60	0.04
BF42	<0.1	20	1.25	42	0.5	2	1.4	3.3	<5	0.53	<0.02
BF43	4.5	48	2.52	75	2.2	5	3.9	6.2	9	0.44	0.1

Note: See Figure 4 for sample positions. TOC—total organic carbon; TS—total sulfur.
*Mass spectrometry.
†Portable gamma-ray spectrometry.
§Mercury analyzer.
#Rockeval.

TABLE 3. PYRITE FRAMBOID SIZE DISTRIBUTIONS FROM THE DEGERBÖLS AND LINDSTRÖM FORMATIONS AT BORUP FIORD

Sample	*n*	Mean diameter (μm)	Standard deviation	Minimum diameter (μm)	Maximum diameter (μm)
BF2	57	7.3	2.4	3	14
BF4	65	6.1	2.2	2	11.5
BF6	102	5.8	2.9	2	19
BF8	105	6.8	2.7	3	21
BF11	96	7.0	2.8	3	20
BF12	102	5.8	1.9	2.5	14
BF13	83	6.2	2.3	3	15
BF13b	109	6.0	1.7	3	13
BF14	122	5.6	1.9	1.5	11.5
BF15	100	6.1	2.3	2.5	20
BF16	49	7.8	2.9	4	18
BF18	103	7.3	2.2	3.5	14
BF20	0	N/A	N/A	N/A	N/A
BF22	1	N/A	N/A	11.5	11.5
BF25	102	7.0	2.2	3	14.5
BF27	103	6.9	3.7	2.5	30
BF28	103	5.8	2.4	3	20
BF30	101	6.3	2.3	2.5	21
BF32	7	N/A	N/A	5	20
BF34	51	7.0	2.3	2.5	14
BF35	107	5.9	3.2	2	20.5
BF36	0	N/A	N/A	N/A	N/A
BF38	0	N/A	N/A	N/A	N/A
BF40	0	N/A	N/A	N/A	N/A

Note: See Figure 4 for sample positions; *n*—number of framboids counted per sample; N/A—not applicable.

Of the 24 samples examined under SEM, 18 had common framboids, while 6 had few or no framboids (Table 3). The smallest framboid populations occurred in levels enriched in redox-sensitive trace metals (e.g., those with Mo/Al > 0.5, V/Al > 30, and U/Th ~ 1; Fig. 4). Samples from the white limestone and chert beds in the basal part of the section (BF40, BF38, and BF36) did not yield framboids. Above this level, small framboids became common between 18 m and 37 m (samples BF35 to BF25), where they had mean diameters between 5.8 μm and 7.0 μm. Framboids were found to be absent from the overlying 20 m of cherty limestones and white cherts, before returning in abundance from the level of BF18 through the remainder of the Degerböls Formation and up to the top of the Lindström Formation (58 m to 96 m section height). Mean framboid diameters through this interval ranged from 5.6 μm to 7.8 μm. The smallest-sized framboid populations in the sequence were found around the extinction level in samples BF14 to BF12, where they attained mean diameters of 5.6 μm and 5.8 μm, respectively (Table 3; Fig. 4). These populations plot in the euxinic-anoxic fields defined by the distribution of framboids in modern sediments (Fig. 7; e.g., Wilkin et al., 1996).

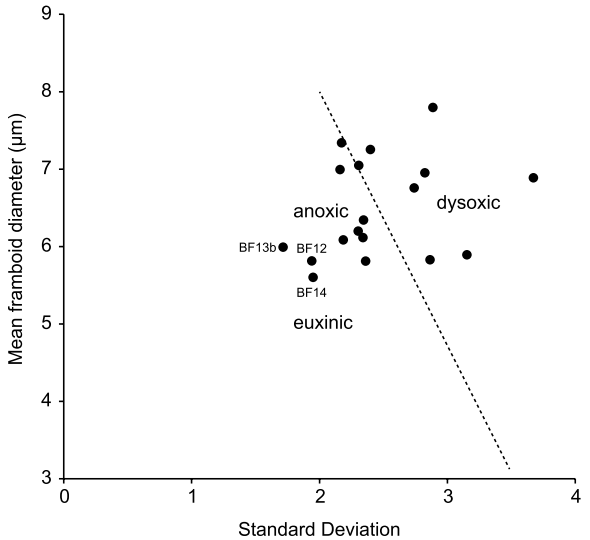

Figure 7. Plot of mean framboid diameter vs. standard deviation for Borup Fiord samples. The separation of the euxinic-anoxic field from the anoxic-dysoxic field is based on data from modern environments that span this range of oxygenation regimes (Bond and Wignall, 2010). Numbers represent sample levels shown in Figure 4.

Mercury, TOC, and TS

Mercury concentrations were generally low throughout the section, but some levels of notable enrichment were found. Samples from the lower meters of the section were below the limit of detection (<5 ppb Hg). However, two intervals recorded significant Hg content: samples BF32 to BF25 (Hg up to 18 ppb) and samples BF15 to BF13b (Hg up to 12 ppb, around the extinction level; Table 2; Fig. 4). Mercury was present in all analyzed samples above the extinction level (BF13b to BF 2), where it varied in concentration between 5 ppb and 10 ppb; the highest postextinction values were found in the topmost meters of the Lindström Formation (Fig. 4). TOC values throughout the section were remarkably consistent, ranging from 0.37% (BF21) to 0.66% (BF35 and BF8). The mean of TOC values in our samples was 0.49%, with a standard deviation of 0.08. The consistency of the TOC values in our samples means that the Hg-enriched intervals described above were still present after normalization. Thus, samples BF32 to BF25 had Hg/TOC values of 13.3–36.3 ppb/wt%, and samples from BF15 to the top of the section varied between 9.0 and 22.3 ppb/wt% (the highest of these being at the extinction level).

It can also be informative to normalize mercury to aluminum, as is standard for the redox-sensitive metals Mo and V (Fig. 4). In modern aquatic settings, Hg has been found to accumulate in sediments as organic compounds, sulfides, and/or oxides following various pathways dependent on the oxidation state of Hg, inorganic and organic complexation of Hg, the presence of humic substances and sulfides, and pH (Ullrich et al., 2001). In contrast, aluminum is not actively involved in these reaction pathways and might therefore be an appropriate chemical species for normalizing mercury (Sanei et al., 2012; Sial et al., 2013). Our Al-normalized data followed a similar pattern to Hg/TOC, with the exception that the highest Hg/Al values occurred at, or immediately after, the extinction level in samples BF13b and BF13 (Hg/Al of 11.3 and 14.1 ppb/wt%, respectively; Fig. 4). Intriguingly, sample BF13b also recorded the highest Mn concentration of the entire sequence (214 ppm; Table 2; Fig. 4); the origin of this Mn spike is discussed below.

TS values were found to be low in the basal 15 m of the section (≤0.05% or below the limit of detection at 0.02%) before rising to modest values (0.02% to a maximum of 0.55% in sample BF29; Table 2). The mean of TS values in our samples was 0.16%, with a standard deviation of 0.13. We also normalized Hg to sulfur to evaluate whether the Hg spike was driven by sulfide drawdown under increased anoxic

conditions rather than enhanced loading of Hg to the basin (e.g., Sanei et al., 2012; Them et al., 2019). While Hg/TS was generally <50 ppb/wt% through most of the succession, there was a clear peak where values rose markedly to >100 ppb/wt% between samples BF15 and BF13, and a further peak of ~100 ppb/wt% was found in the topmost meters of the Permian part of the section (samples BF4 to BF2). The highest value was 219 ppb/wt% in sample BF13b, precisely at the Capitanian extinction level (Fig. 4).

The clearest signals in this data set are that: (1) both Hg/TOC and Hg/Al were higher in sediments that also recorded elevated concentrations of redox-sensitive trace metals and abundant populations of small pyrite framboids (BF32 to BF25 and BF15 upward); and (2) Hg/TS showed a clear peak around the Capitanian extinction level, where it was around twice as high as the next-most-enriched interval.

Carbon Isotopes

The $\delta^{13}C_{org}$ values from Borup Fiord were generally very stable around –25‰ to –26‰ (Fig. 4), except in the interval between 10 m and 30 m height, where values fluctuated between –23‰ and –28‰ in a double positive-negative shift (although the first positive shift of this pair was recorded by only one sample). The uppermost ~18 m section of the Lindström Formation showed a gradual shift toward lighter $\delta^{13}C_{org}$ values, from –25‰ to –27‰. This probably represents the onset of the prominent negative carbon isotope shift seen across the Permian-Triassic boundary observed in the Sverdrup Basin (Grasby et al., 2011) and globally (e.g., Holser et al., 1991; Holser and Magaritz, 1995; Wignall et al., 1998).

DISCUSSION

Boreal-Wide Capitanian Extinction

Brachiopods are common and diverse taxa in the Borup Fiord succession, where, alongside bryozoans, they are the dominant benthos. Both groups disappear abruptly around 32 m below the Lindström–Blind Fiord formational contact, at a level that also sees the cessation of carbonate deposition (which we interpret to be the Degerböls-Lindström contact), a feature that is also seen in Greenland and Spitsbergen (Bond et al., 2015). No brachiopods are found above this extinction level within the Permian succession at Borup Fiord, indicating a severe crisis for shelly benthos, although a low-diversity population of brachiopods and bryozoans persisted into the early part of the Changhsingian elsewhere in Arctic Canada (Beauchamp, 1994; Baud et al., 2008). The loss of brachiopods and bryozoans is not a function of facies: These fauna are found in cherts below the extinction level, and this facies type dominates above that level. The extinction clearly had less impact on the burrowing fauna because intense *Zoophycos* bioturbation persists across the extinction horizon up to the latest Permian.

What was the extinction timing? In the absence of biostratigraphically useful taxa such as conodonts, regional and global correlation of the extinction losses relies on chemostratigraphic and lithostratigraphic comparisons. The Borup Fiord section is remarkably similar, lithologically, to age-equivalent strata in Spitsbergen, which lay (paleogeographically) ~1000 km to the northeast. In both localities, the Middle to Late Permian succession is dominated by a succession of cherts and cherty limestones with a few thin limestone beds (Fig. 8), and the main extinction of shelly benthos coincides with the end of Permian carbonate deposition. At Borup Fiord, the extinction level is 32 m below the latest Permian formational contact; at the Festningen section in Spitsbergen, it is 40 m below the Kapp Starostin–Vardebukta formational contact (Fig. 8; Bond et al., 2015).

Comparison of the $\delta^{13}C_{org}$ record from Borup Fiord with that from Festningen (Bond et al. 2015) revealed similar patterns in $\delta^{13}C_{org}$ values (Fig. 8), in which shifts toward light or heavy values occur at approximately the same distance beneath the latest Permian formational contacts. These include a prominent negative excursion in both sections (larger at Borup Fiord), which is followed by a positive-negative couplet in both (again, larger at Borup Fiord) and then a long, stable interval with $\delta^{13}C_{org}$ values around –25‰ in the ~25–30 m of strata leading up to the extinction. The extinction level itself is marked by a small, brief, positive-negative couplet in the order of 1‰–2‰ at Borup Fiord and Festningen. Following the extinction, there is a gradual positive excursion through 15–20 m of strata, succeeded by a gradual negative shift over a similar distance up to the top of the cherts that mark the respective formational contacts in both sections (Fig. 8). The similarity of these records implies contemporaneous extinction losses in both regions. Our $\delta^{13}C_{org}$ record is not sufficiently resolved to permit detailed chemostratigraphic correlation with more distant regions, but it is notable that the Capitanian extinction is also associated with carbon isotope shifts of similar magnitudes in Tethys (China; e.g., Wignall et al., 2009a; Bond et al., 2010b) and Panthalassa (Japan; Isozaki et al., 2007). This suggests widespread destabilization of the carbon cycle through the Capitanian extinction interval.

East Greenland (the Wandel Sea Basin, which lay ~1000 km southeast of the Sverdrup Basin) provides additional support for a Boreal-wide Capitanian crisis. There, abundant and diverse brachiopods and bryozoans disappear at the top of the Wegener Halvø Formation (Stemmerik, 2001), and the overlying Schuchert Dal Formation contains a depauperate fauna (Sørensen et al., 2007). The age of this formational contact is unclear, but the most recent conodont work on the Ravnefjeld Formation (an offshore lateral equivalent of the Wegener Halvø Formation) identified mesogondolellids of intra-Capitanian age (e.g., Nielsen and Shen, 2004; Sørensen et al., 2007; Legler and Schneider, 2008). This suggests that the brachiopod and bryozoan losses at the top of the Wegener Halvø Formation record a mid- to late Capitanian crisis. Taken together, the lithostratigraphic similarities, $\delta^{13}C_{org}$ record, and limited biostratigraphic data suggest that a synchronous annihilation of shelly benthic faunas occurred across the Boreal Realm within the Capitanian Stage.

Causes of the Capitanian Extinction

A causal role for marine anoxia in the Capitanian extinction has been tentatively suggested (Clapham and Bottjer, 2007; Clapham et al., 2009) on the basis that taxa more tolerant of oxygen stress (i.e., mollusks) replaced the brachiopods as the dominant shelly benthos in the extinction aftermath. Pyrite petrographic and trace metal data from Borup Fiord (Figs. 4 and 7) provide clear evidence that the extinction coincided with the deterioration of seafloor oxygenation, lending support to an anoxia kill hypothesis in higher latitudes. In addition to an increase in Mo, V, and U concentrations and a proliferation of small pyrite framboids, the extinction level at Borup Fiord also shows a marked increase in Mn. Manganese (II) is soluble in anoxic waters but precipitates as a "bathtub ring" where the redox boundary intercepts the seafloor (Frakes and Bolton, 1984). The Mn enrichment at Borup Fiord therefore implies that anoxic conditions were developed in the deeper waters of the Sverdrup Basin at the time of extinction. Age-equivalent strata in Spitsbergen record a remarkably similar redox history, in which the main extinction event coincided with a phase of oxygen-poor deposition (Bond et al., 2015). Bioturbation persists through the extinction horizon in both Ellesmere Island and Spitsbergen, indicating that full seafloor anoxia did not develop; instead, our geochemical proxies suggest that dysoxia, which is lethal for most benthos, was the likely kill mechanism in the Boreal Realm.

The role of acidification in the Capitanian crisis finds support in the record from higher-latitude

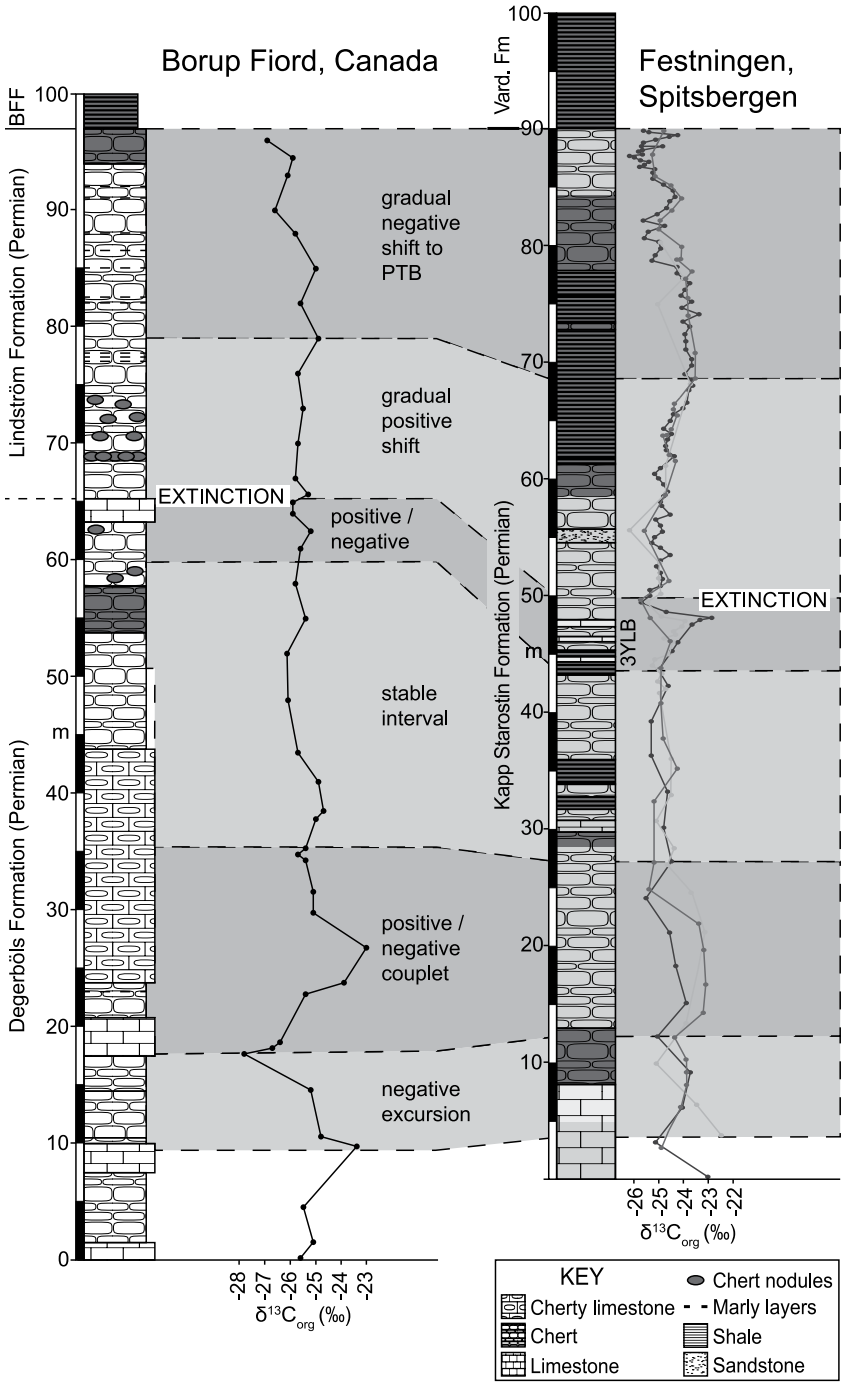

Figure 8. Lithostratigraphic and chemostratigraphic correlation of the Borup Fiord section with Kapp Starostin on Spitsbergen (78.0950°N, 13.8240°E; after Bond et al., 2015), showing the Degerböls and Lindström Formations up to contact with the overlying Blind Fiord Formation (BFF, Canada) and the Kapp Starostin Formation up to the contact with the overlying Vardebukta Formation (Vard. Fm). The Permian-Triassic boundary (PTB) lies a few meters above this formational contact in both areas. Colors in the lithology column indicate white, pale-gray, dark-gray, and yellow beds. The three organic carbon isotope ($\delta^{13}C_{org}$) curves from Spitsbergen were generated in Erlangen (red and green circles) and Calgary (blue circles). In both locations, the brachiopod extinction is associated with a small (1‰–2‰) positive-negative carbon isotope couplet and occurs in strata around 32 m (Canada) and 40 m (Spitsbergen) below the prominent formational contact, which is used as a tie point here.

regions (which are more susceptible because of the greater solubility of CO_2 in colder waters; Beauchamp and Grasby, 2012; Bond et al., 2015). Thus, the brachiopod losses coincide with the cessation of carbonate deposition in the Boreal Realm, and limestones are rare above the extinction level in the Lindström Formation in Arctic Canada, the Kapp Starostin Formation in Spitsbergen, and the Wegener Halvø Formation in East Greenland. These observations are consistent with ocean acidification being a driver for the Capitanian crisis in cooler-water settings, but testing awaits a reliable deep-time pH proxy.

Climate change (both cooling and warming) has been implicated in the Capitanian crisis, and the observation that the extinction was equally abrupt but more severe for brachiopods in the Boreal Realm (100% at Borup Fiord; 87% in Spitsbergen) and high southerly latitude Gondwanan realms (Shi and Shen, 2000; Shen and Shi, 2002, 2004) than in the Paleoequatorial Realm (Shen and Shi, 1996, 2002) suggests that warming is at least partly implicated in the crisis. Marine organisms living in warmer (lower-latitude) regions generally have higher thermal limits than those living in cooler (higher-latitude) regions (for a summary, see Song et al., 2014).

Ultimate Cause of Extinction: Is Mercury Enrichment a Proxy for Emeishan Volcanism?

Our mercury record provides a tentative link between the Boreal brachiopod extinction and distant volcanism in the Emeishan Traps of southwest China, where the onset of eruptions was coincident with mass extinction in that region (Wignall et al., 2009a). Thus, there are two clear spikes in Hg/TOC and Hg/Al, the second and largest of which coincides with the loss of brachiopods and cessation of carbonate deposition. The Sverdrup Basin was very far removed from South China, but it is not inconceivable that mercury was transported this great distance by atmospheric processes, including the strong midlatitude stratospheric winds invoked by Grasby et al. (2011) for latest Permian mercury anomalies in the region. The concentrations of Hg in our samples were relatively small (up to 20 ppb), perhaps due to the distance between the site of Hg deposition and its potential source area in China. Interestingly, Hg/TOC also rises abruptly to around 100 ppb/wt% at the Capitanian extinction level in Spitsbergen (Grasby et al., 2016). This is significantly higher than values we recorded in the Sverdrup Basin (~40 ppb/wt%), but it again illustrates a similar pattern of Hg enrichment coincident with extinction.

It is also noteworthy that our Hg anomalies—normalized to both TOC and Al—occur

at dysoxic levels (i.e., 18–38 m section height and around the extinction level), suggesting either that Hg concentrations increased during oxygen-poor deposition or that there was a common cause. Thus, the Hg enrichments seen at Borup Fiord might be a product of distant volcanism (which induces oxygen restriction through warming), a function of local anoxia, or, of course both. However, the Hg/TS record has a clear peak around the extinction level, where it is around twice as high as the next-most-enriched interval. This suggests that the Hg spike is decoupled from effects of redox on Hg concentrations and reflects enhanced loading of Hg to the basin, because Hg/TS is significantly lower in the strata between 18 and 38 m section height, which we also interpret to have been deposited under dysoxic conditions. In their assessment of marine Ordovician-Silurian boundary successions in South China, Shen et al. (2019) found mercury to be overwhelmingly associated with pyrite, and they suggested that Hg concentrations should be normalized to total sulfur (as a proxy for pyrite). The fact that our Hg spike at the extinction level withstands normalization thus supports a volcanic origin. Intriguingly, the Hg/TS spike in the topmost meters of the Lindström Formation might be a tantalizing record of the onset of eruptions in the Siberian Traps. Unfortunately, study of the Permian-Triassic extinction in our Borup Fiord section is hindered by poor exposure of the basalmost shales of the Blind Fiord Formation.

Given our overall observations, we envisage a volcanogenic extinction scenario for the Boreal Realm in which the distant Emeishan Traps drove oxygen depletion by driving global warming (see compilations that reveal the Capitanian as an interval of accelerating warming—Korte et al., 2008; Chen et al., 2013; Song et al., 2019). Warming in turn enhanced stratification of the water column, leading to the deadly expansion of oxygen minimum zones into shelf habitats. The Capitanian extinction increasingly appears to have been a global crisis on par with the "Big 5" of the Phanerozoic, and, as with the other mass extinctions from the time of Pangea, it had its origins in volcanism.

CONCLUSIONS

A diverse and abundant benthic fauna, dominated by brachiopods and bioturbators such as *Zoophycos* trace makers, was found in the Middle to Late Permian Degerböls and Lindström Formations of the Sverdrup Basin. The brachiopods, but not the burrowers, went abruptly extinct at a level interpreted to be of intra-Capitanian age, and the younger Permian strata are devoid of shelly fauna. Redox proxies (Mo, V, and U and pyrite framboid populations) indicate that the extinction level coincides with oxygen-poor (dysoxic) deposition, while Mn enrichment suggests that more intensely anoxic conditions occurred in contemporaneous, deeper waters.

This Boreal Capitanian extinction record strengthens the case for this crisis being a global event rather than one confined to equatorial waters. In South China, the extinction coincided closely with the eruption of the Emeishan flood basalts (Wignall et al., 2009a), and the associated enrichment of Hg (and Hg/Al and Hg/TOC values) in the Sverdrup record further supports this link. The Hg peak also coincides with the development of dysoxic conditions (which could have been driven by volcanogenic climate change), making it difficult to disentangle whether the enrichment directly records volcanism or the changes driven by the volcanism.

ACKNOWLEDGMENTS

We thank Benoit Beauchamp for helpful discussions about the stratigraphy of Ellesmere Island, and Sara Pruss and Haijun Song for constructive reviews of this manuscript. Field work was supported through the Geological Survey of Canada's High Arctic Large Igneous Province (HALIP) project, within the GEM Program. We thank the Natural Environment Research Council, UK for additional financial support (grant NE/J01799X/1 to Bond). Natural Resources Canada's Polar Continental Shelf Program (PCSP) in Resolute Bay, Nunavut, provided valuable logistical support. Deirdra Stacey provided field assistance. Mark Anderson prepared thin sections and polished chips, and Tony Sinclair assisted with scanning electron microscope work in Hull. Finally, we thank the pilots of Kenn Borek Air and Universal Helicopters Newfoundland and Labrador for providing safe passage around the Arctic, and the staff of Eureka Weather Station for their hospitality.

REFERENCES CITED

Balkwill, H.R., 1978, Evolution of Sverdrup Basin: Arctic Canada: American Association of Petroleum Geologists Bulletin, v. 62, p. 1004–1028.

Baud, A., Nakrem, H.A., Beauchamp, B., Beatty, T., Embry, A.F., and Henderson, C.M.B., 2008, Lower Triassic bryozoan beds from Ellesmere Island, High Arctic, Canada: Polar Research, v. 27, p. 428–440, https://doi.org/10.1111/j.1751-8369.2008.00071.x.

Beauchamp, B., 1994, Permian climatic cooling in the Canadian Arctic, *in* Klein, G.O., ed., Pangea: Paleoclimate, Tectonics, and Sedimentation during Accretion, Zenith, and Breakup of a Supercontinent: Geological Society of America Special Paper 288, p. 229–246, https://doi.org/10.1130/SPE288-p229.

Beauchamp, B., and Grasby, S.E., 2012, Permian lysocline shoaling and ocean acidification along NW Pangea led to carbonate eradication and chert expansion: Palaeogeography, Palaeoclimatology, Palaeoecology, v. 350, p. 73–90, https://doi.org/10.1016/j.palaeo.2012.06.014.

Beauchamp, B., Henderson, C.M.B., Grasby, S.E., Gates, L., Beatty, T., Utting, J., and James, N.P., 2009, Late Permian sedimentation in the Sverdrup Basin, Canadian Arctic: The Lindström and Black Stripe formations: Canadian Society of Petroleum Geology Bulletin, v. 57, p. 167–191, https://doi.org/10.2113/gscpgbull.57.2.167.

Bond, D.P.G., and Grasby, S.E., 2017, On the causes of mass extinctions: Palaeogeography, Palaeoclimatology, Palaeoecology, v. 478, p. 3–29, https://doi.org/10.1016/j.palaeo.2016.11.005.

Bond, D.P.G., and Wignall, P.B., 2010, Pyrite framboid study of marine Permo-Triassic boundary sections: A complex anoxic event and its relationship to contemporaneous mass extinction: Geological Society of America Bulletin, v. 122, p. 1265–1279, https://doi.org/10.1130/B30042.1.

Bond, D.P.G., and Wignall, P.B., 2014, Large igneous provinces and mass extinctions: An update, *in* Keller, G., and Kerr, A.C., eds., Volcanism, Impacts, and Mass Extinctions: Causes and Effects: Geological Society of America Special Paper 505, p. 29–55, https://doi.org/10.1130/2014.2505(02).

Bond, D.P.G., Hilton, J., Wignall, P.B., Ali, J.R., Stevens, L.G., Sun, Y.-D., and Lai, X.-L., 2010a, The Middle Permian (Capitanian) mass extinction on land and in the oceans: Earth-Science Reviews, v. 102, p. 100–116, https://doi.org/10.1016/j.earscirev.2010.07.004.

Bond, D.P.G., Wignall, P.B., Wang, W., Védrine, S., Jiang, H.-S., Lai, X.-L., Sun, Y.-D., Newton, R.J., Cope, H., and Izon, G., 2010b, The mid-Capitanian (Middle Permian) mass extinction and carbon isotope record of South China: Palaeogeography, Palaeoclimatology, Palaeoecology, v. 292, p. 282–294, https://doi.org/10.1016/j.palaeo.2010.03.056.

Bond, D.P.G., Wignall, P.B., Joachimski, M.M., Sun, Y.-D., Savov, I., Grasby, S.E., Beauchamp, B., and Blomeier, D.P.G., 2015, An abrupt extinction in the Middle Permian (Capitanian) of the Boreal Realm (Spitsbergen) and its link to anoxia and acidification: Geological Society of America Bulletin, v. 127, p. 1411–1421, https://doi.org/10.1130/B31216.1.

Chen, B., Joachimski, M.M., Shen, S.Z., Lambert, L.L., Lai, X.L., Wang, X.D., Chen, J., and Yuan, D.X., 2013, Permian ice volume and palaeoclimate history: Oxygen isotope proxies revisited: Gondwana Research, v. 24, p. 77–89, https://doi.org/10.1016/j.gr.2012.07.007.

Chen, F.Y., Xue, W.Q., Yan, J.X., Wignall, P.B., Meng, Q., Luo, J.X., and Feng, Q.L., 2018, Alatoconchids: Giant Permian bivalves from South China: Earth-Science Reviews, v. 179, p. 147–167, https://doi.org/10.1016/j.earscirev.2018.01.012.

Clapham, M.E., and Bottjer, D.J., 2007, Permian marine paleoecology and its implications for large-scale decoupling of brachiopod and bivalve abundance and diversity during the Lopingian (Late Permian): Palaeogeography, Palaeoclimatology, Palaeoecology, v. 249, p. 283–301, https://doi.org/10.1016/j.palaeo.2007.02.003.

Clapham, M.E., Shen, S.-Z., and Bottjer, D.J., 2009, The double mass extinction revisited: Reassessing the severity, selectivity, and causes of the end-Guadalupian biotic crisis (Late Permian): Paleobiology, v. 35, p. 32–50, https://doi.org/10.1666/08033.1.

Embry, A.F., 1988, Triassic sea-level changes: Evidence from the Canadian Arctic Archipelago, *in* Wilgus, C.K., Hastings, B.S., Kendall, C.G.St.C., Posamentier, H.W., Ross, C.A., and Van Wagoner, J.C., eds., Sea-Level Changes: An Integrated Approach: Society of Economic Paleontologists and Mineralogists (SEPM) Special Publication 42, p. 249–259, https://doi.org/10.2110/pec.88.01.0249.

Embry, A.F., 1989, Correlation of Upper Palaeozoic and Mesozoic sequences between Svalbard, Canadian Arctic Archipelago, and northern Alaska, *in* Collinson, J.D., ed., Correlation in Hydrocarbon Exploration: Dordrecht, Netherlands, Springer, p. 89–98, https://doi.org/10.1007/978-94-009-1149-9_9.

Embry, A.F., and Beauchamp, B., 2008, Sverdrup Basin, *in* Miall, A.D., ed., The Sedimentary Basins of United States and Canada: Elsevier, p. 451–472, https://doi.org/10.1016/S1874-5997(08)00013-0.

Embry, A.F., and Beauchamp, B., 2019, Sverdrup Basin, *in* Miall, A.D., ed., The Sedimentary Basins of Unites States and Canada: Elsevier, p. 559–592, https://doi.org/10.1016/B978-0-444-63895-3.00014-0.

Font, E., Adatte, T., Sial, A.N., Drude de Lacerda, L., Keller, G., and Punekar, J., 2016, Mercury anomaly, Deccan volcanism, and the end-Cretaceous mass extinction:

Geology, v. 44, p. 171–174, https://doi.org/10.1130/G37451.1.

Frakes, L.A., and Bolton, B.R., 1984, Origin of manganese giants: Sea-level change and anoxic-oxic history: Geology, v. 12, p. 83–86, https://doi.org/10.1130/0091-7613(1984)12<83:OOMGSC>2.0.CO;2.

Grasby, S.E., and Beauchamp, B., 2008, Intrabasin variability of the carbon-isotope record across the Permian-Triassic transition, Sverdrup Basin, Arctic Canada: Chemical Geology, v. 253, p. 141–150, https://doi.org/10.1016/j.chemgeo.2008.05.005.

Grasby, S.E., Sanei, H., and Beauchamp, B., 2011, Catastrophic dispersion of coal fly ash into oceans during the latest Permian extinction: Nature Geoscience, v. 4, p. 104–107, https://doi.org/10.1038/ngeo1069.

Grasby, S.E., Beauchamp, B., Embry, A.F., and Sanei, H., 2013, Recurrent Early Triassic ocean anoxia: Geology, v. 41, p. 175–178, https://doi.org/10.1130/G33599.1.

Grasby, S.E., Beauchamp, B., Bond, D.P.G., Wignall, P., Talavera, C., Galloway, J.M., Piepjohn, K., Reinhardt, L., and Blomeier, D., 2015, Progressive environmental deterioration in northwestern Pangea leading to the latest Permian extinction: Geological Society of America Bulletin, v. 127, p. 1331–1347, https://doi.org/10.1130/B31197.1.

Grasby, S.E., Beauchamp, B., Bond, D.P.G., Wignall, P.B., and Sanei, H., 2016, Mercury anomalies associated with three extinction events (Capitanian crisis, latest Permian extinction and the Smithian/Spathian extinction) in NW Pangea: Geological Magazine, v. 153, p. 285–297, https://doi.org/10.1017/S0016756815000436.

Groves, J.R., and Wang, Y., 2013, Timing and size selectivity of the Guadalupian (Middle Permian) fusulinoidean extinction: Journal of Paleontology, v. 87, p. 183–196, https://doi.org/10.1666/12-076R.1.

Hall, G., and Pelchat, P., 1997, Evaluation of a direct solid sampling atomic absorption spectrometer for the trace determination of mercury in geological samples: Analyst (London), v. 122, p. 921–924, https://doi.org/10.1039/a700194k.

Harrison, J.C., Mayr, U., McNeil, D.H., Sweet, A.R., McIntyre, D.J., Eberle, J.J., Harington, C.R., Chalmers, J.A., Dam, G., and Nohr-Hansen, H., 1999, Correlation of Cenozoic sequences of the Canadian Arctic region and Greenland; implications for the tectonic history of northern North America: Bulletin of Canadian Petroleum Geology, v. 47, p. 223–254.

Holser, W.T., and Magaritz, M., 1995, The Late Permian carbon isotope anomaly in the Bellerophon Basin, Carnic and Dolomite Alps: Jahrbuch der Geologischen Bundesanstalt, v. 128, p. 75–82.

Holser, W.T., Schönlaub, H.P., Boeckelmann, K., Magaritz, M., and Orth, C.J., 1991, The Permian-Triassic of the Gartnerkofel-1 core (Carnic Alps, Austria): Synthesis and conclusions: Abhandlungen der Geologischen Bundesanstalt, v. 45, p. 213–235.

Huang, Y.G., Chen, Z.Q., Wignall, P.B., Grasby, S.E., Zhao, L.S., Wang, X.D., and Kaiho, K., 2019, Biotic responses to volatile volcanism and environmental stresses over the Guadalupian-Lopingian (Permian) transition: Geology, v. 47, p. 175–178, https://doi.org/10.1130/G45283.1.

Isozaki, Y., Kawahata, H., and Ota, A., 2007, A unique carbon isotope record across the Guadalupian-Lopingian (Middle-Upper Permian) boundary in mid-oceanic paleoatoll carbonates: The high-productivity "Kamura event" and its collapse in Panthalassa: Global and Planetary Change, v. 55, p. 21–38, https://doi.org/10.1016/j.gloplacha.2006.06.006.

Jin, Y.-G., Zhang, J., and Shang, Q.-H., 1994, Two phases of the end-Permian mass extinction, *in* Embry, A.F., Beauchamp, B., and Glass, D.J., eds., Pangea: Global Environments and Resources: Canadian Society of Petroleum Geologists Memoir 17, p. 813–822.

Korte, C., Jones, P.J., Brand, U., Mertmann, D., and Veizer, J., 2008, Oxygen isotope values from high-latitudes: Clues for Permian sea-surface temperature gradients and late Palaeozoic deglaciation: Palaeogeography, Palaeoclimatology, Palaeoecology, v. 269, p. 1–16, https://doi.org/10.1016/j.palaeo.2008.06.012.

Lafargue, E., Espitalité, J., Marquis, F., and Pillot, D., 1998, Rock-Eval 6 applications in hydrocarbon exploration, production and soil contamination studies: Revue de l'Institut Français du Pétrole, v. 53, no. 4, p. 421–437, https://doi.org/10.2516/ogst:1998036.

Legler, B., and Schneider, J.W., 2008, Marine ingressions into the Middle/Late Permian saline lake of the southern Permian Basin (Rotliegend, northern Germany) possibly linked to sea-level highstands in the Arctic rift system: Palaeogeography, Palaeoclimatology, Palaeoecology, v. 267, p. 102–114, https://doi.org/10.1016/j.palaeo.2008.06.009.

McGhee, G.R., Clapham, M.E., Sheehan, P.M., Bottjer, D.J., and Droser, M.L., 2013, A new ecological-severity ranking of major Phanerozoic biodiversity crises: Palaeogeography, Palaeoclimatology, Palaeoecology, v. 370, p. 260–270, https://doi.org/10.1016/j.palaeo.2012.12.019.

Nielsen, J.K., and Shen, Y., 2004, Evidence for sulfidic deep water during the Late Permian in the East Greenland Basin: Geology, v. 32, p. 1037–1040, https://doi.org/10.1130/G20987.1.

Payne, J.L., and Clapham, M.E., 2012, End-Permian mass extinction in the oceans: An ancient analog for the twenty-first century?: Annual Review of Earth and Planetary Sciences, v. 40, p. 89–111, https://doi.org/10.1146/annurev-earth-042711-105329.

Percival, L.M., Ruhl, M., Hesselbo, S.P., Jenkyns, H.C., Mather, T.A., and Whiteside, J.H., 2017, Mercury evidence for pulsed volcanism during the end-Triassic mass extinction: Proceedings of the National Academy of Sciences of the United States of America, v. 114, p. 7929–7934, https://doi.org/10.1073/pnas.1705378114.

Proemse, B.C., Grasby, S.E., Wieser, M.E., Mayer, B., and Beauchamp, B., 2013, Molybdenum isotopic evidence for oxic marine conditions during the latest Permian extinction: Geology, v. 41, p. 967–970, https://doi.org/10.1130/G34466.1.

Sanei, H., Grasby, S.E., and Beauchamp, B., 2012, Latest Permian mercury anomalies: Geology, v. 40, p. 63–66, https://doi.org/10.1130/G32596.1.

Shen, J., Algeo, T.J., Chen, J., Planavsky, N.J., Feng, Q., Yu, J., and Liu, J., 2019, Mercury in marine Ordovician/Silurian boundary sections of South China is sulfide-hosted and non-volcanic in origin: Earth and Planetary Science Letters, v. 511, p. 130–140, https://doi.org/10.1016/j.epsl.2019.01.028.

Shen, S.-Z., and Shi, G.-R., 1996, Diversity and extinction patterns of Permian brachiopods of South China: Historical Biology, v. 12, p. 93–110, https://doi.org/10.1080/08912969609386558.

Shen, S.-Z., and Shi, G.-R., 2002, Paleobiogeographical extinction patterns of Permian brachiopods in the Asian–western Pacific region: Paleobiology, v. 28, p. 449–463, https://doi.org/10.1666/0094-8373(2002)028<0449:PEPOPB>2.0.CO;2.

Shen, S.-Z., and Shi, G.-R., 2004, Capitanian (late Guadalupian, Permian) global brachiopod palaeobiogeography and latitudinal diversity pattern: Palaeogeography, Palaeoclimatology, Palaeoecology, v. 208, p. 235–262, https://doi.org/10.1016/j.palaeo.2004.03.009.

Shen, S.-Z., and Shi, G.-R., 2009, Latest Guadalupian brachiopods from the Guadalupian/Lopingian boundary GSSP section at Penglaitan in Laibin, Guangxi, South China, and implications for the timing of the pre-Lopingian crisis: Palaeoworld, v. 18, p. 152–161, https://doi.org/10.1016/j.palwor.2009.04.010.

Shi, G.-R., and Shen, S.-Z., 2000, Asian–western Pacific Permian brachiopods in space and time, *in* Yin, H.-F., Dickens, J.M., Shi, G.-R., and Tong, J.-N., eds., Permian–Triassic Evolution of Tethys and Western Circum-Pacific: Amsterdam, Netherlands, Elsevier, p. 327–352, https://doi.org/10.1016/S0920-5446(00)80019-9.

Sial, A.N., Lacerda, L.D., Ferreira, V.P., Frei, R., Marquillas, R.A., Barbosa, J.A., Gaucher, C., Windmöller, C.C., and Pereira, N.S., 2013, Mercury as a proxy for volcanic activity during extreme environmental turnover: The Cretaceous-Paleogene transition: Palaeogeography, Palaeoclimatology, Palaeoecology, v. 387, p. 153–164, https://doi.org/10.1016/j.palaeo.2013.07.019.

Sial, A.N., Chen, J., Lacerda, L.D., Peralta, S., Gaucher, C., Frei, R., Cirilli, S., Ferreira, V.P., Marquillas, R.A., Barbosa, J.A., Pereira, N.S., and Belmino, I.K.C., 2014, High-resolution Hg chemostratigraphy: A contribution to the distinction of chemical fingerprints of the Deccan volcanism and Cretaceous-Paleogene boundary impact event: Palaeogeography, Palaeoclimatology, Palaeoecology, v. 414, p. 98–115, https://doi.org/10.1016/j.palaeo.2014.08.013.

Silva, M.V.N., Sial, A.N., Barbosa, J.A., Ferreira, V.P., Neumann, V.H., and De Lacerda, L.D., 2013, Carbon isotopes, rare-earth elements and mercury geochemistry across the K-T transition of the Paraíba Basin, northeastern Brazil, *in* Bojar, A.-V., et al., eds., Isotopic Studies in Cretaceous Research: Geological Society [London] Special Publication 382, p. 85–104, https://doi.org/10.1144/SP382.2.

Song, H., Wignall, P.B., Chu, D., Tong, J., Sun, Y., Song, H., He, W., and Tian, L., 2014, Anoxia/high temperature double whammy during the Permian-Triassic marine crisis and its aftermath: Scientific Reports, v. 4, p. 4132, https://doi.org/10.1038/srep04132.

Song, H., Wignall, P.B., Song, H., Dai, X., and Chu, D., 2019, Seawater temperature and dissolved oxygen over the past 500 million years: Journal of Earth Science, v. 30, p. 236–243, https://doi.org/10.1007/s12583-018-1002-2.

Sørensen, A.M., Håkansson, E., and Stemmerik, L., 2007, Faunal migration into the Late Permian Zechstein basin—Evidence from bryozoan palaeobiogeography: Palaeogeography, Palaeoclimatology, Palaeoecology, v. 251, p. 198–209, https://doi.org/10.1016/j.palaeo.2007.03.045.

Stanley, S.M., 2016, Estimates of the magnitudes of major marine mass extinctions in Earth history: Proceedings of the National Academy of Sciences of the United States of America, v. 113, p. E6325–E6334, https://doi.org/10.1073/pnas.1613094113.

Stanley, S.M., and Yang, X., 1994, A double mass extinction at the end of the Paleozoic Era: Science, v. 266, p. 1340–1344, https://doi.org/10.1126/science.266.5189.1340.

Stemmerik, L., 2001, Stratigraphy of the Upper Permian Wegener Halvø Formation, Karstryggen area, East Greenland—A low productivity carbonate platform: Sedimentology, v. 48, p. 79–97, https://doi.org/10.1046/j.1365-3091.2001.00352.x.

Them, T.R., II, Jagoe, C.H., Caruthers, A.H., Gill, B.C., Grasby, S.E., Gröcke, D.R., Yin, R., and Owens, J.D., 2019, Terrestrial sources as the primary delivery mechanism of mercury to the oceans across the Toarcian oceanic anoxic event (Early Jurassic): Earth and Planetary Science Letters, v. 507, p. 62–72, https://doi.org/10.1016/j.epsl.2018.11.029.

Thibodeau, A.M., Ritterbush, K., Yager, J.A., West, A.J., Ibarra, Y., Bottjer, D.J., Berelson, W.M., Bergquist, B.A., and Corsetti, F.A., 2016, Mercury anomalies and the timing of biotic recovery following the end-Triassic mass extinction: Nature Communications, v. 7, p. 11147, https://doi.org/10.1038/ncomms11147.

Ullrich, S.M., Tanton, T.W., and Abdrashitova, S.A., 2001, Mercury in the aquatic environment: A review of factors affecting methylation: Critical Reviews in Environmental Science and Technology, v. 31, p. 241–293, https://doi.org/10.1080/20016491089226.

Wang, X.-D., and Sugiyama, T., 2000, Diversity and extinction patterns of Permian coral faunas of China: Lethaia, v. 33, p. 285–294, https://doi.org/10.1080/00241160750053853.

Weidlich, O., 2002, Permian reefs re-examined: Extrinsic control mechanisms of gradual and abrupt changes during 40 my of reef evolution: Geobios, v. 35, p. 287–294, https://doi.org/10.1016/S0016-6995(02)00066-9.

Wignall, P.B., 2001, Large igneous provinces and mass extinctions: Earth-Science Reviews, v. 53, p. 1–33, https://doi.org/10.1016/S0012-8252(00)00037-4.

Wignall, P.B., Morante, R., and Newton, R., 1998, The Permo-Triassic transition in Spitsbergen: $\delta^{13}C_{org}$, chemostratigraphy, Fe and S geochemistry, facies, fauna and trace fossils: Geological Magazine, v. 135, p. 47–62, https://doi.org/10.1017/S0016756897008121.

Wignall, P.B., Sun, Y., Bond, D.P.G., Izon, G., Newton, R.J., Védrine, S., Widdowson, M., Ali, J.R., Lai, X., Jiang, H., and Cope, H., 2009a, Volcanism, mass extinction, and carbon isotope fluctuations in the Middle Permian of China: Science, v. 324, p. 1179–1182, https://doi.org/10.1126/science.1171956.

Wignall, P.B., Védrine, S., Bond, D.P.G., Wang, W., Lai, X.L., Ali, J.R., and Jiang, H.S., 2009b, Facies analysis and sea-level change at the Guadalupian-Lopingian global stratotype (Laibin, South China), and its bearing on the end-Guadalupian mass extinction: Journal of the Geological Society [London], v. 166, p. 655–666, https://doi.org/10.1144/0016-76492008-118.

Wilkin, R.T., Barnes, H.L., and Brantley, S.L., 1996, The size distribution of framboidal pyrite in modern sediments: An indicator of redox conditions: Geochimica et Cosmochimica Acta, v. 60, p. 3897–3912, https://doi.org/10.1016/0016-7037(96)00209-8.

Yang, X.-N., Shi, G.-J., Liu, J.-R., Chen, Y.-T., and Zhou, J.-P., 2000, Inter-taxa differences in extinction process of Maokouan (Middle Permian) fusulinaceans: Science in China, ser. D, v. 43, p. 633–637, https://doi.org/10.1007/BF02879507.

Science Editor: Bradley S. Singer
Associate Editor: Christian Koeberl

Manuscript Received 5 March 2019
Revised Manuscript Received 21 May 2019
Manuscript Accepted 20 June 2019

Printed in the USA